Journal of Luminescence 132 (2012) 391–397

Contents lists available at SciVerse ScienceDirect

Journal of Luminescence

journal homepage: www.elsevier.com/locate/jlumin

Comparative study of the spectroscopic properties of Yb^{3+}/Er^{3+} codoped tellurite glasses modified with R_2O (R=Li, Na and K)

H. Desirena, E. De la Rosa*, V.H. Romero, J.F. Castillo, L.A. Díaz-Torres, J.R. Oliva

Centro de Investigaciones en Optica, A. P.1-948, León, Gto. 37150, Mexico

ARTICLE INFO

Article history:
Received 15 April 2011
Received in revised form
3 August 2011
Accepted 24 August 2011
Available online 31 August 2011

Keywords:
Upconversion
Er^{3+}/Yb^{3+}
Judd–Ofelt
Energy transfer
Tellurite glasses
Decay time

ABSTRACT

Spectroscopic characterization of Yb^{3+}/Er^{3+} codoped TeO_2–R_2O–ZnO–Ln_2O_3 glasses as a function of network modifiers (R=Li, Na and K) has been investigated. The Judd–Ofelt parameters (Ω_t), quantum efficiency in near infrared (1.55 μm) and visible up-conversion (546 and 660 nm) and quality factor spectroscopy (χ) were calculated. Three up-conversion emission bands centered at 525, 546 and 660 nm were observed as maxima for glasses containing potassium. The measured lifetime of $^4I_{13/2}$, $^4F_{9/2}$ and $^4S_{3/2}$ from Er^{3+} and $^4F_{5/2}$ from Yb^{3+} levels increased when potassium (K) replaced lithium (Li) and Na. The maximum emission cross-section (ECS) for $^4I_{13/2}\rightarrow{}^4I_{15/2}$ transition of Er^{3+} was calculated to be 1.02×10^{-20} cm^2 for TeO_2–Li_2O–ZnO–Ln_2O_3 glasses. The energy transfer efficiency (ET) from Yb^{3+} to Er^{3+}, $(^4F_{5/2})+(^4I_{15/2})\rightarrow(^4F_{7/2})+(^4I_{13/2})$, was calculated using the measured lifetimes of Yb^{3+} with and without the presence of acceptor (Er^{3+}). The maximum calculated ET was 58% for 0.25 mol% of Er^{3+} and 3 mol% of Yb^{3+} for TeO_2–K_2O–ZnO–Ln_2O_3 glass composition.

1. Introduction

There is an enormous interest in the luminescence properties of Yb^{3+}/Er^{3+} codoped glasses for fiber optic lasers and amplifiers [1–4]. The main interest on this system is based on the requirement to get high efficiency and broad bandwidth for fiber amplifiers at 1.55 μm. The efficiency of such emission depends on dopant concentration and the phonon energy of the host that in turn depends on the glass composition. Typically, Er^{3+} doped glasses are pumped with a laser diode (LD) at 970 nm, promoting population from $^4I_{15/2}$ to $^4I_{11/2}$. For a host with a high phonon energy, the population on $^4I_{11/2}$ decays very fast non-radiatively to $^4I_{13/2}$, from where it decays radiatively (1.55 μm) to ground state. The fast depopulation of $^4I_{11/2}$ avoids the promotion to upper levels, thereby avoiding the upconversion emission and back transfer to Yb^{3+} when it is present. A good example for this kind of host is phosphate glasses with phonon energy of 1100 cm^{-1}. However, if the phonon energy is very high a deleterious effect is observed on the spectroscopic properties of the main transition. This is the case of borate glasses with phonon energy of 1350 cm^{-1} [5]. Recently, the interest on tellurite glasses as a host for Er^{3+} ions has increased, in part because of the large increase up to ~70 nm in bandwidth, which is about three times larger than that obtained from silica and phosphate glasses [6–9]. However, the low phonon energy of this kind of glasses (750 cm^{-1}) promotes cooperative phenomena such as upconversion (UC) process that is the major drawback for the eyes-safe emission. Although the presence of UC is deleterious for 1.55 μm emission, it can find many useful applications in visible lasers, displays, lighting, security and many others.

Lots of work on tellurite glasses have been reported by different authors. There, the spectroscopic properties of Er^{3+} as functions of glass composition and ion concentration have been studied [10–15]. The optical, mechanical and chemical properties of the host depend on its composition and hence, the selection of glass components is very important in the development of high performance tellurite glass. Several network modifiers have been studied, but only a few works have been reported to characterize the effect of alkalis. Alkalis are well-known modifiers widely used in phosphate glasses, where spectroscopic, optical and thermo-mechanical properties have been modified [16–18]. It has been reported that the addition of Na_2O improves the solubility of rare earth, opening the possibility to use high concentration of dopants, which is very important in the design of high efficiency short length fiber amplifiers [19]. Recently, we have systematically characterized the optical and thermo-mechanical properties of alkali metals and found that the use of Li_2O in tellurite glasses is more favorable. Here in this work, we report the spectroscopic properties of Er^{3+}/Yb^{3+} codoped TeO_2–ZnO–R_2O–Ln_2O_3 glasses as a function of the alkali R=Li, Na, K and Yb^{3+} concentration. The Judd–Ofelt intensity parameters were calculated and used to analyze spectroscopic properties such as radiative transition probabilities, cross-sections,

* Corresponding author. Tel.: +52 477 441 4200; fax: +52 477 441 4209.
E-mail addresses: elder@cio.mx, hagdes@cio.mx (E. De la Rosa).

0022-2313/$ - see front matter © 2011 Elsevier B.V. All rights reserved.
doi:10.1016/j.jlumin.2011.08.041

fluorescence branching ratio, radiative lifetime, fluorescence lifetime and quality factor as a function of the alkali metal used. We also analyzed the dependence of upconversion as functions of both alkalis and Yb^{3+} concentration.

2. Experimental

The glass composition was $74TeO_2$–$12.75ZnO$–$10R_2O$–$(3-x)La_2O_3$–$0.25Er_2O_3$–xYb_2O_3 (mol%), where R=Li, Na and K and $x=1, 2, 3$. All samples were prepared from the starting chemical constituent tellurite oxide (TeO_2), zinc oxide (ZnO), lithium oxide (Li_2O), sodium carbonate (Na_2CO_3), potassium carbonate (K_2CO_3), erbium oxide (Er_2O_3), ytterbium oxide (Yb_2O_3) and lanthanum oxide (La_2O_3). All reactants were of analytical grade and used as received. Calculated quantities of precursors were mixed in a glass dish and melted in an electric furnace at 900 °C for 1 h in platinum crucibles so that a homogeneously mixed melt was obtained. The melt was cast into a suitable aluminum mold kept at 300 °C. The obtained glasses were subsequently annealed at temperature from 300 °C to 350 °C depending on glass composition. The time to finish the annealing process took around 22 h. The samples were polished to optical quality and only bubble and streak free samples were taken for optical measurements. The density of each sample was measured by the Archimedes method using distilled water as immersion liquid. Samples were cut and polished to 2 mm thick slabs for different measurements. The transmission spectra were measured using a spectrophotometer (Perkin–Elmer Lambda 900) in the range of 300–1700 nm. The refractive index of the samples was measured at 632.8 by a prism coupler (Metricon, Model 2010). The emission spectra were recorded by exciting the samples at 970 nm with a low power AlGaAs laser diode. The signal emitted was focused into an Acton Research SP-2357 monochromator and detected by InGaAs detector (Thorlabs DET10C) and photomultiplier tube (Acton Research PD471). The decay profile corresponding to 556, 660 and 1532 nm was recorded using a SR540 chopper (Stanford Research System) connecting the photodetector directly to an oscilloscope (Tektronix TDS 3025B). All the optical measurements were performed at room temperature.

3. Results and discussion

3.1. Judd–Ofelt parameters

The Judd–Ofelt parameters were calculated considering ten absorption bands of Er^{3+}/Yb^{3+} co-doped TeO_2–ZnO–R_2O–Ln_2O_3 glasses from the spectrum shown in Fig. 1. The measured absorption line strength (S_{meas}) for the induced electric dipole transition of each band was determined experimentally from the area under the absorption band and can be expressed in terms of absorption coefficient α by the equation:

$$S_{meas}(J\rightarrow J') = \frac{3ch(2J+1)}{8\pi^3\lambda e^2 N_0}\left[\frac{9n}{(n^2+2)^2}\right]\int \alpha(\lambda)\,d\lambda. \quad (1)$$

Here, J and J' denote the total angular momentum quantum number of the initial and final states, respectively, e is the charge of the electron, c the velocity of light in vacuum, h the Planck constant, λ is the mean wavelength of the absorption band (nm) and N_o is the Er^{3+} ion concentration per unit volume (ions/cm^3). $\alpha(\lambda)=2.303D_0(\lambda)/d$ is the measured absorption coefficient at a given wavelength λ (nm/cm), $D_0(\lambda)$ the optical density [$\log I/I_0$], d the thickness of the sample (cm) and n is the measured refractive index. The measured values of S_{meas} obtained by the numerical integration of the absorption line shapes were used to obtain the

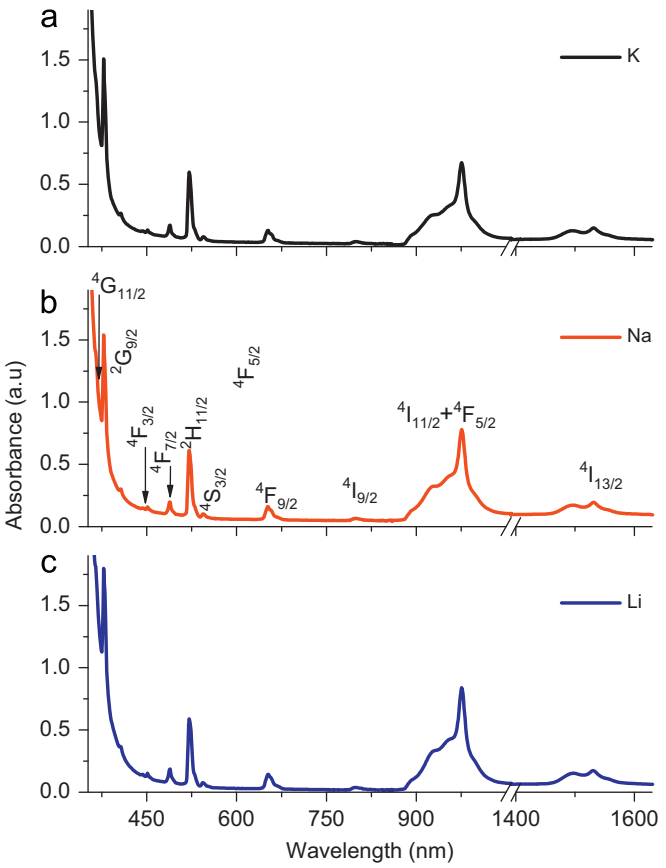

Fig. 1. Absorption spectrum of Er^{3+}/Yb^{3+} codoped tellurite glasses containing (a) Li, (b) Na and (c) K.

phenomenological Judd–Ofelt (JO) parameters Ω_t by fitting the experimental value with the theoretical expression derived by Judd [20] and Ofelt [21]:

$$S_{ed}(J\rightarrow J') = \sum_{t=2,4,6}\Omega_t |\langle (S,L)J||U^{(t)}||S',L')J'\rangle|^2. \quad (2)$$

Here, $U^{(t)}$ are the doubly reduced matrix elements of the unit tensor operator of rank $t=2$, 4 and 6, which are calculated from the intermediate coupling approximation. The reduced matrix elements are virtually independent of the ligand species surrounding the rare earth (RE^{3+}) ions and thus approximately unchanged from host to host. Ω_2, Ω_4 and Ω_6 are the phenomenological JO parameters; they exhibit the influence of the host on the radiative transition probabilities, since they contain implicitly the effect of the odd-symmetry crystal field terms. Thus, the changes presented by these parameters are consequence of the changes in the host composition due to the substitution of modifiers (Li, Na and K), as shown in Fig. 2. The Ω_2 parameter is closely related to the hypersensitive transitions, i.e., the larger the line strength of the hypersensitive transition, the larger the value of Ω_2. It is well known that hypersensitivity is related to the covalency parameter through the nephelauxetic effect and it is attributed to the increased polarizability of the ligands around the rare earth ions. Higher ligand polarizability results in a larger overlap between rare earth and ligands orbital, i.e., higher degree of covalency between rare earth ion and the ligands. The value of Ω_2 is also affected by the asymmetry of the rare earth sites, that is reflected in the crystal field parameter [22,23]; therefore large values of Ω_2 parameter mean large asymmetry of tellurite glasses. The Ω_6 parameter is inversely proportional to the covalency of the Er–O bond and Ω_4 is

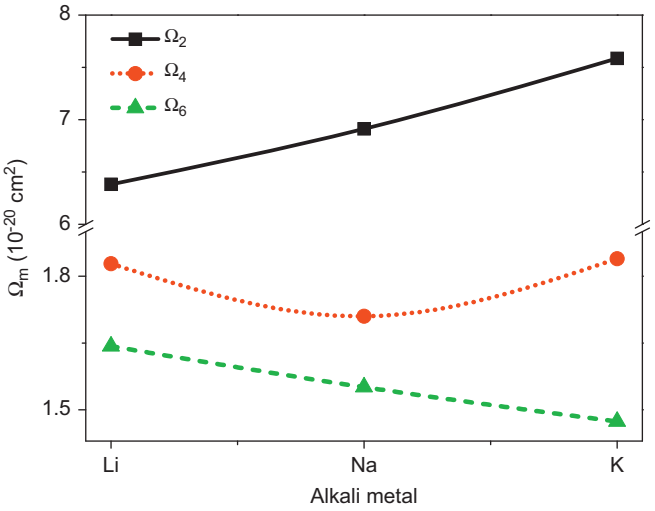

Fig. 2. JO parameters as a function of network modifiers.

affected by factors causing the changes of Ω_2 and Ω_6 [24]. According to the electronegativity theory [25], the smaller the difference of eletronegativity between cations and anions, the stronger the covalency of the bond. Since the values of electronegativity for K, Na, Li and O are 0.8, 0.9, 1.0 and 3.5, respectively, it is expected that the covalency of Li–O bond is stronger than those of Na–O and K–O bonds. Therefore, with the replacement of Li by K and Na, it is expected that the electrons from oxygen are more available for coordination with Er^{3+}. Then, the covalency of Er–O bond is increased and their effect is reflected directly in the values of Ω_2 and Ω_6 parameter, as shown in Fig. 2. In order to elucidate this effect, the covalency parameter based on hypersensitive transition was determined. Such transition must have a large value of the doubly reduced matrix elements $|\langle (S,L)J||U^{(t)}||(S',L')J'\rangle|^2$ and obeys the selection rules $|\Delta J| \leq 2, |\Delta L| \leq 2$ and $\Delta S = 2$. The $^4I_{15/2} \rightarrow {}^2H_{11/2}$ transition of Er^{3+} is known as hypersensitive transition and he peak wavelength is used directly as a parameter reflecting the covalency of the Er–O bond [26]. Thus, the intensity of line strengths (S_{meas}) was calculated and the results were found to be 5.840×10^{-20}, 6.106×10^{-20} and 6.665×10^{-20} cm^2 for Li, Na and K, respectively. The obtained result confirms that the covalency of Er–O bond increases gradually with the replacement of network modifiers in the order Li → Na → K.

For those transitions with $\Delta J = 1$, there would be a contribution of the magnetic dipole transition (S_{md}). The $^4I_{13/2} \rightarrow {}^4I_{15/2}$ transition of Er^{3+} meets this requirement and the line strength is partly a contribution of S_{md} and partly of electric-dipole transition S_{ed} [27]. The S_{md} contribution corresponds to 30% in silicate glasses as has been reported and explains the narrow emission band of such transition [28]. Therefore, it is necessary to increase the electric-dipole transition in order to get broad band and flat emission spectra, that are very useful in optical amplifiers [22]. According to the Judd–Ofelt theory, the line strength of S_{ed} components of the $^4I_{13/2} \rightarrow {}^4I_{15/2}$ transition is given by[29]

$$S_{ed}[{}^4I_{13/2}; {}^4I_{15/2}] = 0.019\Omega_2 + 0.118\Omega_4 + 1.462\Omega_6, \quad (3)$$

where the coefficients of Ω_t parameters are the reduced matrix elements of the unit tensor operator, $U^{(t)}$, which can be found in the literature [30]. From this equation, it is clear that the Ω_6 parameter is much more significant for the value of S_{ed} due to the largest coefficient. Therefore, an increment in the Ω_6 value necessarily means an increment of the band width of $^4I_{13/2} \rightarrow {}^4I_{15/2}$ transition and confirms that the broad band increases as the Ω_6 coefficient increases. The largest coefficient was obtained for the alkali with the lowest ionic radii as shown in Fig. 2 and will be discussed later in Section 3.3. The complete procedure to obtain the JO parameters and some spectroscopic properties in Er^{3+} doped tellurite glasses and other host has been described elsewhere [31,32]. The obtained JO parameters follow the typical behavior $\Omega_2 > \Omega_4 > \Omega_6$ and are in agreement with results reported recently for various glass compositions, as shown in Table 1. In addition, by taking the ratio $\chi = \Omega_4/\Omega_6$ named as the spectroscopic quality factor it is possible to predict the behavior of various lasing transitions in a given matrix uniquely represented by Ω_4 and Ω_6 parameters [35]. This value is inversely proportional to the intensity of the laser transition, and a small value of this parameter means more intense laser emission. For our samples, χ shows a minimum value of 1.09 for glasses containing K and increases to 1.14 and 1.16 for Na and Li, respectively. These values are smaller than those reported recently for other tellurite glass composition as displayed in Table 1 [33,34].

Using the Ω_t parameters, the radiative transition probability (A_{rad}) from different upper states to the corresponding lower manifold states can be evaluated from the relation

$$A_{rad}[(S,L)J; (S',L')J'] = \frac{64\pi^4 e^3}{3h(2J+1)\lambda^3}\left[\frac{n(n^2+2)^2}{9}S_{ed} + n^3 S_{md}\right]. \quad (4)$$

Here, S_{ed} and S_{md} represent the predicted fluorescence line strength for the induced electric and magnetic dipole transition, respectively. S_{ed} is calculated using Eq. (2) and presents a host dependence through the Ω_t parameters. S_{md}, ignored here, can be calculated with the expression

$$S_{md} = \left(\frac{e^2h^2}{16\pi^2m^2c^2}\right)|\langle (S,L)J||L+2S||(S',L')J'\rangle|^2. \quad (5)$$

The values of the radiative transition probability for $^4S_{3/2} \rightarrow {}^4I_{15/2}$, $^4F_{9/2} \rightarrow {}^4I_{15/2}$ and $^4I_{13/2} \rightarrow {}^4I_{15/2}$ transitions for the different network modifiers under study are shown in Table 2. The radiative transition probability is proportional to the refractive index of the glass host according to the relation $A_{rad} \propto n(n^2+2)^2$. From Table 2 a decreasing tendency was observed in every transition in the order K → Na → Li, which is mainly because of the increase of refractive index with replacement of K by Li and Na. The total radiative transition probability A_T also permits calculation of the radiative lifetime τ_{rad} for an excited state J using the expression

$$\tau_{rad} = A_T^{-1} = \left\{\sum_{S',L',J'} A[(S,L)J; (S';L')J']\right\}^{-1}. \quad (6)$$

Because the total radiative transition probability depends of Ω_t parameters the radiative decay time is inversely proportional to a linear combination of these JO parameters. The radiative

Table 1
JO parameters for various tellurite glass compositions.

Glass composition	Ω_2 (10^{-20} cm^2)	Ω_4 (10^{-20} cm^2)	Ω_6 (10^{-20} cm^2)	χ
TeO_2–WO_3–Bi_2O_3[a]	6.06	1.57	0.95	1.65
TeO_2–Nb_2O_5–Na_2O[b]	6.86	1.53	1.12	1.36
TeO_2–ZnO–K_2O[c]	7.58	1.83	1.47	1.09
TeO_2–ZnO–Na_2O[c]	6.91	1.71	1.55	1.14
TeO_2–ZnO–Li_2O[c]	6.38	1.82	1.64	1.16

[a] Ref. [34].
[b] Ref. [35].
[c] Reported in this paper.

Table 2
Fluorescence lifetime (τ_{exp}), radiative transition probability and quantum efficiency (QE) as functions of rare earth concentration and network modifiers.

	Er/Yb (mol%)	τ_{exp} (ms)			QE (%)			A_{rad} (s^{-1})		
		$^4S_{3/2}$	$^4F_{9/2}$	$^4I_{13/2}$	$^4S_{3/2}$	$^4F_{9/2}$	$^4I_{13/2}$	$^4S_{3/2}$	$^4F_{9/2}$	$^4I_{13/2}$
Li	0.25/1	0.185	0.269	3.83	84	100	100	4593	3717	278
	0.25/2	0.180	0.260	4.33	82	96	100			
	0.25/3	0.167	0.237	4.41	76	88	100			
Na	0.25/1	0.187	0.271	4.04	78	88	100	4207	3272	247
	0.25/2	0.180	0.267	4.23	75	87	100			
	0.25/3	0.177	0.249	4.4	74	81	100			
K	0.25/1	0.195	0.279	4.13	71	88	93	3678	3166	226
	0.25/2	0.182	0.269	4.37	66	85	99			
	0.25/3	0.175	0.264	4.85	64	83	100			

transition probability also depends on the local field correction at the Er^{3+} site, showing a dependence on the refractive index.

3.2. Absorption (ACS) and emission cross-section (ECS).

The cross sections quantify the ion ability to absorb or emit light; large emission cross-section means high gain coefficient and low threshold energy of laser pump. Thus, in order to obtain the best performance of laser and optical amplifiers, it is necessary to improve the emission cross-section as high as possible. The absorption cross-section of the $^4I_{13/2}\rightarrow{}^4I_{15/2}$ (1.53 μm) transition of Er^{3+} has been determined from the absorption spectra of Er^{3+}/Yb^{3+} codoped tellurite glasses, using the equation

$$\sigma_a = \frac{2.303\log(I_0/I)}{NL}. \quad (7)$$

where $\log(I_0/I)$ is the optical density, L is the sample thickness and N is the concentration of Er^{3+} ion. The emission cross-section was obtained according to the McCumber theory from the expression [36]

$$\sigma_e(\nu) = \sigma_a(\nu)\exp[(\varepsilon - h(c/\lambda))/kT], \quad (8)$$

where ν is the photon frequency, ε is the net free energy required to excite one erbium ion from the $^4I_{15/2}$ to the $^4I_{13/2}$ level at temperature T, h is the Planck's constant, k is the Boltzmann constant and c is the light velocity in vacuum; ε was estimated using the approximation provided in Ref. [37], and the obtained value is $\varepsilon = 6554\ cm^{-1}$. In this case, three basic assumptions are considered: (1) the Stark levels for a given manifold are equally spaced, $E_{ij}=(j-1)E_i$, with a degeneracy equal to 7 and 8 for $^4I_{13/2}$ and $^4I_{15/2}$, respectively; (2) E_0 is the energy between the two levels and was calculated taking the average between the absorption and emission peak and (3) E_1 and E_2 are calculated measuring the half width energy calculated from the wavelength peak to the point where signal decreased to 5%. The calculated values of absorption and emission cross-section for Te_2O–La_2O_3–K_2O–ZnO glass are shown in Fig. 3a. The largest emission cross-section of $1.02\times10^{-20}\ cm^2$ was obtained for the glass composition Te_2O–La_2O_3–Li_2O–ZnO and then decreased to $0.97\times10^{-20}\ cm^2$ and $0.92\times10^{-20}\ cm^2$ for Te_2O–La_2O_3–Na_2O–ZnO and Te_2O–La_2O_3–K_2O–ZnO composition, respectively, (see Fig. 3b). Since the emission cross-section is proportional to the refractive index of the host, $\sigma_e \propto (n^2+2)^2/n$, and the refractive index increases in the order K→Na→Li, it is expected that the Te_2O–La_2O_3–Li_2O–ZnO glass has the largest emission cross-section among the alkali. The calculated values of emission cross-section reported here are in agreement with results reported recently [34] and are higher than those values reported for silica ($7.9\times10^{-21}\ cm^2$) [38] and phosphate glasses ($6.8\times10^{-21}\ cm^2$) [39].

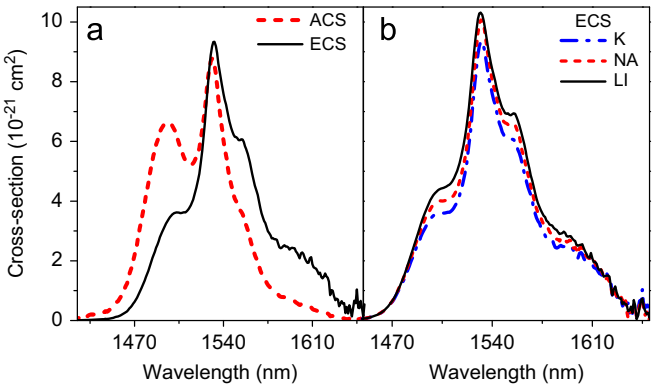

Fig. 3. Cross-section of $^4I_{13/2}\rightarrow{}^4I_{15/2}$ transition (Er^{3+}); (a) absorption cross-section (ACS) and emission cross-section (ECS) of Te_2O–K_2O–ZnO–Ln_2O_3 glass and (b) ECS for different network modifiers (Li, Na and K).

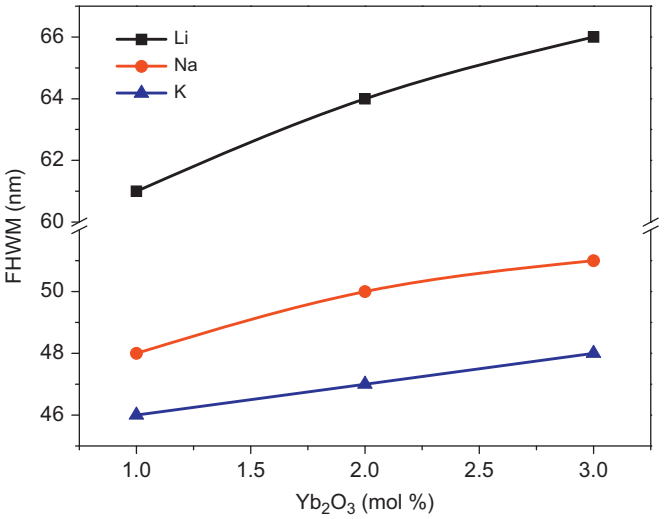

Fig. 4. FWHM of $^4I_{13/2}\rightarrow{}^4I_{15/2}$ transition centered at 1.532 μm as a function of Yb^{3+} concentration for Te_2O–K_2O–ZnO–Ln_2O_3, Te_2O–Na_2O–ZnO–Ln_2O_3 and Te_2O–Li_2O–ZnO–Ln_2O_3 O glasses.

3.3. Fluorescence properties of Er^{3+}/Yb^{3+} codoped tellurite glasses

3.3.1. Infrared and upconversion emission

The well-known NIR emission of Er^{3+} ($^4I_{13/2}\rightarrow{}^4I_{15/2}$) in the Yb^{3+}/Er^{3+} codoped tellurite glasses was observed at 1.532 μm, with a spectral bandwidth ranging from 46 to 66 nm, depending on the concentration of Yb^{3+} ions and the appropriate network modifier, as is shown in Fig. 4. This means an increment of 20 nm in the bandwidth just by controlling the ion concentration and glass composition. The obtained results show a continuous increment of the bandwidth with the increment of Yb^{3+} ion for different host compositions as displayed in Fig. 4. In addition, the ion concentration and glass composition modify the intensity of the signal emitted, showing a maximum at 1 mol% of Yb_2O_3 and increasing a little when K replaced Li and Na as indicated in Fig. 5. Such dependence clearly indicates the importance of the right glass composition and concentration of Er^{3+} and Yb^{3+} ions.

Two strong visible emission bands were also observed as displayed in Fig. 6: the green band associated with the mixed transition $^2H_{11/2}+{}^4S_{3/2}\rightarrow{}^4I_{15/2}$ and centered at 526 and 548 nm, and the red band associated with $^4F_{9/2}\rightarrow{}^4I_{15/2}$ transition and centered at 660 nm. The visible emission is the result of the well-known upconversion process and it depends on the concentration of Yb^{3+} ions. The overall intensity of the upconverted signal

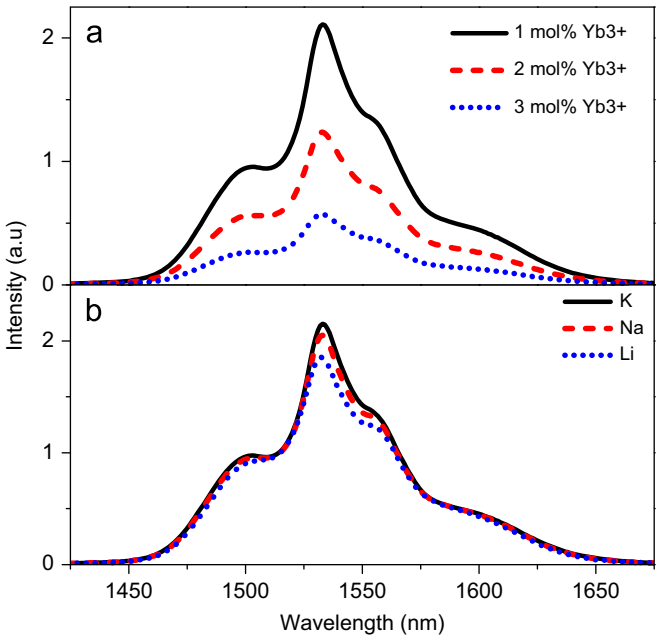

Fig. 5. Emission intensity at 1.532 μm; (a) as a function of Yb^{3+} concentration and (b) as a function of network modifier.

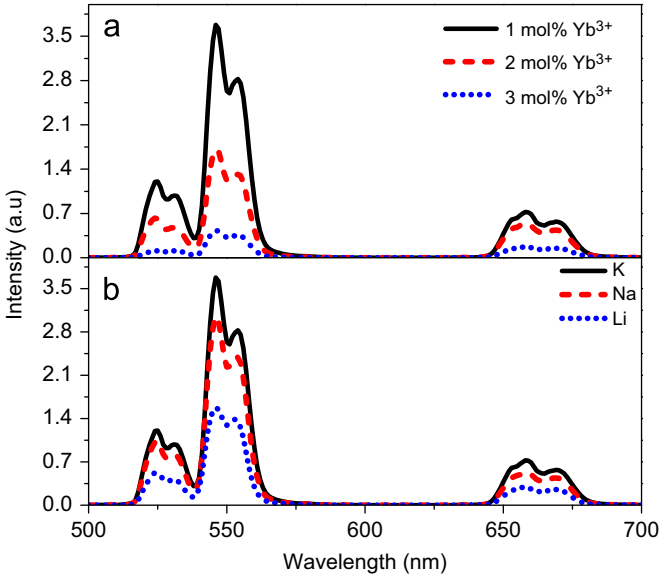

Fig. 6. Upconversion emission intensity of $^4S_{3/2}\rightarrow{}^4I_{15/2}$ and $^4F_{9/2}\rightarrow{}^4I_{15/2}$ transitions; (a) as a function of Yb^{3+} concentration and (b) as a function of network modifier.

shows a maximum at 1 mol% of Yb_2O_3 and after this both green and red bands decrease as indicated in Fig. 6a. The maximum is explained in terms of the energy transfer efficiency due to the right concentration of sensitizer (donors) while the decrement of signal is probably associated with the energy migration between donors (Yb^{3+}) as a result of the high ion concentration. The intensity of the upconverted signals also depends on glass composition, showing an increase in the order Li→Na→K as shown in Fig. 6b. This result suggests an increase of distance between Er^{3+} and Er^{3+}, avoiding the formation of cluster and then the fluorescence quenching. This is supported by the previous results where it was shown that K improves the solubility of Er^{3+} ions. Of course, this behavior is also followed by emission band at 1.532 μm. The visible bands are relaxation pathways contrary to pathways associated with NIR emission, and then the enhancement of the former is deleterious to the very important emission associated with the communication window.

The integrated upconverted (I_{upc}) signal was plotted as a function of the pumping power (I_{pp}) and the experimental data for unsaturated UC process were fitted by the expression $I_{upc}=kI_{pp}^{n}$, where n denotes the number of photons involved in the upconversion process. Fig. 7 shows such a behavior with $n\sim2$ for 1 and 2 mol% of Yb^{3+} for samples containing lithium as a host modifier. The calculated n values were 1.52 and 1.22 for green and red band, respectively, for 1 mol% of Yb^{3+} and reduced to 1.44 and 1.16 for 2 mol% of Yb^{3+}. Such changes suggest the presence of additional processes strongly related with the presence of Yb^{3+}. It can be attributed to the linearization of UC process because of the saturation of $^4I_{13/2}$ and $^4F_{9/2}$ energy levels due to the combined effect of cross-relaxation (CR) according to the equation $Er^{3+}(^2H_{11/2})+Er^{3+}(^4I_{15/2})\rightarrow Er^{3+}(^4I_{9/2})+Er^{3+}(^4I_{13/2})$ and energy transfer process from Yb^{3+} to Er^{3+}. According to this, the possible physical mechanism describing both visible and NIR emissions of Er^{3+}/Yb^{3+} is as follows: Er^{3+} (acceptors) and Yb^{3+} (donor) ions are excited by the pumping signal according to the equation $h\nu+Er^{3+}(^4I_{15/2})\rightarrow Er^{3+}(^4I_{11/2})$ and $h\nu+Yb^{3+}(^4F_{5/2})\rightarrow Yb^{3+}(^4F_{7/2})$, respectively. However, most of the energy is absorbed for the Yb^{3+} ions due to the larger absorption cross-section. A small fraction of Yb^{3+} ions decay radiatively to ground state, leading to emission at 1.03 μm, and partly transfer their energy to the Er^{3+} due to the resonance between $^2F_{7/2}\rightarrow{}^2F_{5/2}$ and $^4I_{15/2}\rightarrow{}^4I_{11/2}$ transitions of Yb^{3+} and Er^{3+}, respectively, as shown in the energy diagram in Fig. 8. The overall result is an increase of population in $^4I_{11/2}$. Part of the populations in $^4I_{11/2}$ relax non-radiatively to $^4I_{13/2}$ level and from here relax to ground state, producing the 1.532 μm emission band, and another part is promoted to $^4F_{7/2}$ by the ET from the relaxation of another excited Yb^{3+} ($^4F_{5/2}\rightarrow{}^4F_{7/2}$) or Er^{3+} ($^4I_{11/2}\rightarrow{}^4I_{15/2}$) ion. Ions excited at $^4F_{7/2}$ decay non-radiatively to $^2H_{11/2}$ and $^4S_{3/2}$ levels due to the phonon energy of the host. From here, the population decays to ground state, producing the green emission centered at 526 nm ($^2H_{11/2}\rightarrow{}^4I_{15/2}$) and 548 nm ($^4S_{3/2}\rightarrow{}^4I_{15/2}$), and partly decays non-radiatively to $^4F_{9/2}$ to finally decays to the ground state, producing the red emission centered at 660 nm ($^4F_{9/2}\rightarrow{}^4I_{15/2}$). Furthermore, part of the population on $^4I_{13/2}$ energy level (populated by non-radiative relaxation from $^4I_{11/2}$ and CR as described above) is re-exited to $^4F_{9/2}$ by the energy transfer from another donor: $Yb^{3+}(^2F_{5/2})+Er^{3+}(^4I_{13/2})\rightarrow Yb^{3+}(^2F_{7/2})+Er^{3+}(^4F_{9/2})$. This mechanism explains the saturation of $^4F_{9/2}$ energy level and the reduced

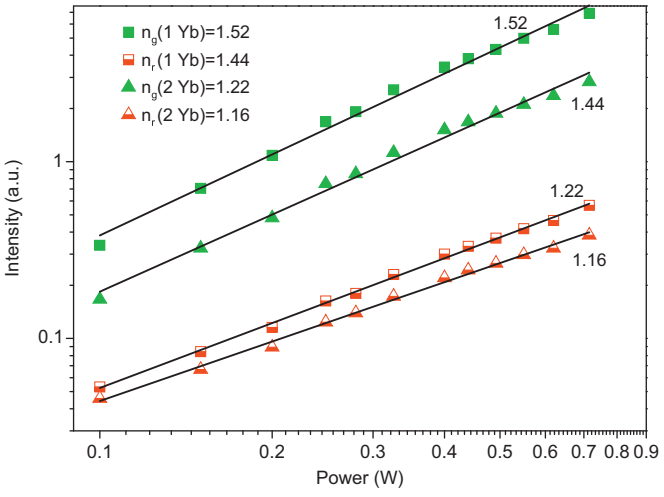

Fig. 7. Pump power dependence of green and red emissions for 0.25 mol% of Er^{3+}, and 1 and 2 mol% of Yb^{3+}.

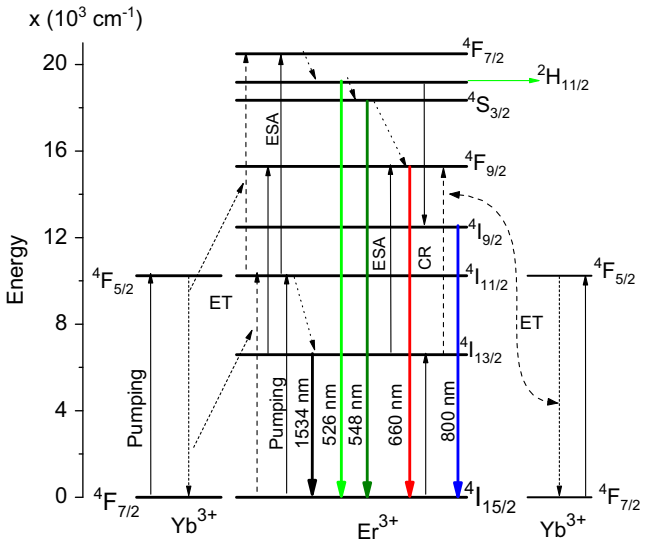

Fig. 8. Energy level diagram of Er^{3+} and Yb^{3+} ions describing the mechanism proposed to explain both visible and infrared emissions.

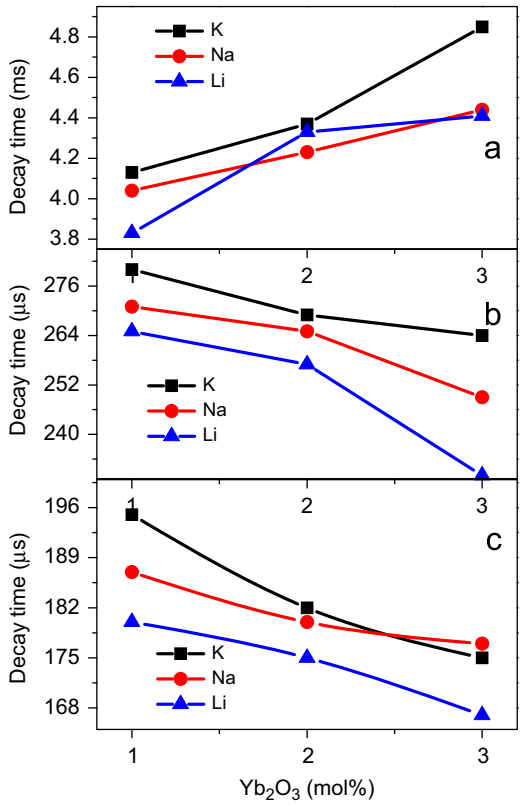

Fig. 9. Fluorescence decay time as a function of Yb^{3+} concentration and network modifiers for (a) $^4I_{13/2}$, (b) $^4S_{3/2}$ and (c) $^4F_{9/2}$ levels.

value of n. The complete mechanism proposed to explain both visible and NIR emissions of Er^{3+}/Yb^{3+} codoped tellurite glasses is described in Fig. 8.

3.3.2. Fluorescence lifetime

The fluorescence decay times of green (560 nm), red (670 nm) and NIR (1.532 μm) emissions for all samples under study are plotted versus Yb^{3+} concentrations in Fig. 9. Such a figure shows the individual effects of each network modifiers and Yb^{3+} concentration. It has been reported that the incorporation of Na to tellurite glasses improves the solubility of rare earth, reducing the fluorescence quenching and increasing decay time (or at least reduce the quenching) with the increase of Er^{3+} concentration [19]. However, our studies show better solubility with the incorporation of K instead of Na, reducing the concentration quenching of Er^{3+} even at higher concentration. The experimental results show an increase of decay time in the order Li, Na and K, indicating that K is the best modifier to improve spectroscopic properties. In addition, the fluorescence decay time of $^4I_{13/2}\rightarrow{}^4I_{15/2}$ transition increases from 3.83 to 4.41 ms for Li, 4.40 to 4.44 ms for Na and 4.13 to 4.85 ms for K when Yb_2O_3 increases from 1 to 3 mol%, as displayed in Fig. 9a. This is partly the result of the higher concentration of sensitizer and the better excitation process of Er^{3+} via the energy transfer from Yb^{3+}, as reported previously [39], and partly the result of a better dispersion of Er^{3+} avoiding cluster formation that in turn avoids fluorescence quenching. The ionic radii of donors and acceptors are similar; as a consequence Yb^{3+} ions can act as a disperser, reducing the cluster formation of Er^{3+}. Fig. 9b and c shows the fluorescence decay time of $^4S_{3/2}$ and $^4F_{9/2}$ energy levels, where a monotonic decrease as a function of Yb^{3+} concentration can be observed. Decay time for green band ranges from 180 to 167 μs, 187 to 174 μs and 195 to 175 μs for Li, Na and K, respectively. For red emission, it ranges from 265 to 230 μs for Li, 271 to 249 μs for Na and 280 to 264 μs for K for different concentrations of Yb^{3+}.

The quantum efficiency (QE) for the three observed transition was calculated using the expression

$$\eta = \tau_{meas}/\tau_{rad}, \tag{9}$$

where τ_{meas} is the experimentally measured lifetime and τ_{rad} is the calculated radiative lifetime obtained from JO parameters. The values of quantum efficiency for all Yb^{3+}/Er^{3+} codoped tellurite glasses are listed in Table 2. The QE of $^4S_{3/2}\rightarrow{}^4I_{15/2}$ transition decreases from 74 to 67% for Li, 67 to 63 for Na and 66 to 59 for K, and for $^4F_{9/2}\rightarrow{}^4I_{15/2}$ transitions it decreases from 100 to 88% for Li, 89 to 81 for Na and 88 to 83% for K when Yb^{3+} concentrations increase from 1 to 3 mol%. In the case of $^4I_{13/2}\rightarrow{}^4I_{15/2}$ transition, quantum efficiency increases slightly from 93 to 100% for K and keeps to 100% for Li and Na.

3.4. Energy transfer in Yb^{3+}/Er^{3+} codoped tellurite glasses

The energy transfer (ET) efficiency from Yb^{3+} to Er^{3+}, $Yb^{3+}(^2F_{5/2})+Er^{3+}(^4I_{15/2})\rightarrow Yb^{3+}(^2F_{7/2})+Er^{3+}(^4I_{11/2})$, can be evaluated, considering no other process than ET, using the expression [40]

$$\eta = 1-\frac{\tau_{Yb\text{-}Er}}{\tau_{Yb}}, \tag{10}$$

where $\tau_{Yb\text{-}Er}$ and τ_{Yb} stand for the fluorescence lifetime of $^2F_{5/2}$ level of codoped Yb^{3+}–Er^{3+} and Yb^{3+} doped glasses, respectively. The ET efficiency increases from 45% to 53% for Li_2O modifier, 51% to 55% for Na_2O and 52% to 58% for K_2O when the Yb^{3+} concentration increases from 1 to 3 mol% as displayed in Fig. 10. Notice the strong effect of host composition increasing ET from 45% for Li to 52% for K at 1 mol% of Yb_2O_3. Since the lifetime of Yb^{3+} (τ_{Yb}) increases from Li to Na and K, it is expected that the maximum ET occurs in glasses containing K. These calculated η values are in agreement with other reports published recently [44], but are lower than those reported for phosphate and silica glasses. It has been reported that ET efficiency from Yb^{3+} to Er^{3+} is mainly dependent on the ratio W_{BT}/W_{MR}, where W_{BT} stands for the energy back transfer efficiency from Er^{3+} ($^4I_{11/2}\rightarrow{}^4I_{15/2}$) to Yb^{3+} ($^2F_{5/2}\rightarrow{}^4F_{7/2}$) and W_{MR} stands for the multi-phonon relaxation $^4I_{11/2}\rightarrow{}^4I_{13/2}$ transition of Er^{3+} [41]. W_{BT} is affected by the lifetime of $^4I_{11/2}$ level of Er^{3+}: large lifetime means large W_{BT}.

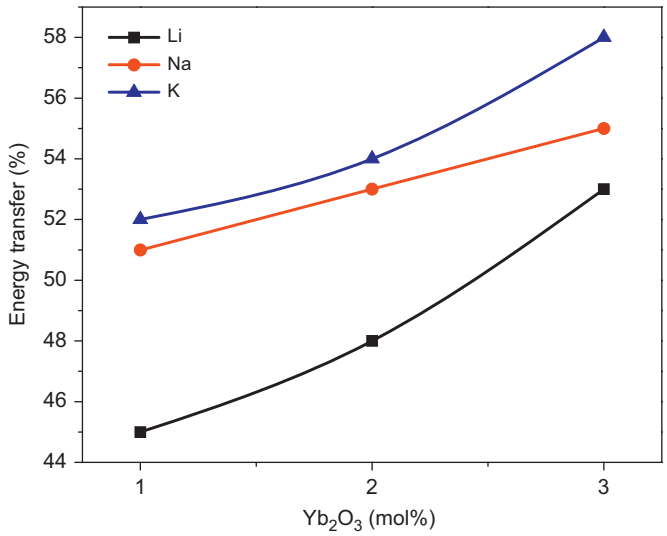

Fig. 10. Glass composition dependence of energy transfer (ET) as a function of Yb^{3+} concentration for K, Na and Li.

For tellurite glasses this value is 140 μs [42], while in silicate and phosphate glasses they are 10 and 1 μs, respectively. In addition, the highest phonon energy of tellurite glasses is around 800 cm^{-1}, while in silicate and phosphate glasses it is around 1000 and 1100 cm^{-1}, respectively [43]. Furthermore, the multiphonon relaxation rate in tellurite glasses is much smaller than in silicate and phosphate glasses. Therefore, low W_{MR} and large W_{BT} mean more time occupied in $^4I_{11/2}$, reducing the ET efficiency in tellurite glasses.

4. Conclusion

Er^{3+}/Yb^{3+} codoped $70TeO_2$–$12.75ZnO$–$10R_2O$–$3.25La_2O_3$ glasses with different network modifiers (R=Li, Na and K) were prepared and the spectroscopic properties as functions of modifiers and Yb^{3+} concentration were analyzed. The Judd–Ofelt analysis shows important changes in the Ω_t parameters by changing the network modifier, these being changes outstanding in the spectroscopic properties of active ions. The σ_e and FWHM of $^4I_{13/2} \rightarrow {}^4I_{15/2}$ transition of Er^{3+} can be increased by changing the network modifier in the order K→Na→Li, the maximum obtained values being 1.02×10^{-20} cm^2 and 66 nm, respectively. However, the presence of K reduces the quenching of Er^{3+} and Yb^{3+}, improving both visible and NIR signals emitted. The concentration of donors plays an important role to improve the energy transfer and then improve the signal emitted. This is also dependent on network modifier, being the maximum for K, and increases with donor concentration. The obtained results suggest that K is the best modifier for applications in laser and optical amplifiers at 1.53 μm emission.

Acknowledgments

This work was partly supported by CONACyT, México, through Grant 134111.

References

[1] A. Mori, Y. Ohishi, S. Sudo, Electron. Lett 33 (1997) 863.
[2] Y. Ohishi, A. Mori, M. Yamada, H. Ono, Y. Nishida, K. Oikawa, Opt. Lett. 23 (1998) 274.
[3] P. Joshi, S. Shen, A. Jha, J. Appl. Phys. 103 (2008) 083543.
[4] S. Shen, A. Jha, X. Liu, M. Naftaly, K. Bindra, H.J. Bookey, A.K. Kar, J. Am. Ceram. Soc. 85 (2002) 1391.
[5] C.B. Layne, W.H. Lowdermilk, M.J. Weber, Phys. Rev. B 16 (1977) 10.
[6] L.L. Neindre, S. Jiang, B.C. Hwang, T. Luo, J. Watson, N. Peyghambarian, J. Non-Cryst. Solids 255 (1999) 97.
[7] J. Li, S. Li, H. Hu, F. Gan, J. Mater. Sci. Technol. 20 (2004) 139.
[8] N.M. Souza Neto, A.Y. Ramos, L.C. Barbosa, J. Non-Cryst. Solids 304 (2002) 195.
[9] X. Shen, Q. Nie, T.F. Xu, Y. Gao, Spectrochim. Acta Part A 61 (2005) 2827.
[10] W.J. Chung, A. Jha, S. Shen, P. Joshi, Philos. Mag. 84 (2004) 1197.
[11] R. El-Mallawany, A. Patra, C.S. Friend, R. Kapoor, P.N. Prasad, Opt. Mater 12 (2004) 34.
[12] H. Lin, G. Meredith, S. Jiang, X. Peng, T. Luo, N. Peyghambarian, E.Y.B. Pun, J. Appl. Phys 93 (2003) 186.
[13] S. Dai, J. Wu, J. Zhang, G. Wang, Z. Jiang, Spectrochim. Acta Part A 62 (2005) 431.
[14] R. Rolli, M. Mongtagna, S. Chaussedent, A. monteil, V.K. Tikhomirov, M. Ferrari, Opt. Mater 21 (2003) 743.
[15] S. Zhao, X Wang, S Xu, L Hu, Chalcogen Lett 2 (2005) 97.
[16] J. Byun, B. Kim, K. Hong, H. Jung, S. Lee, K. Ryoo, A. Izyneev, V.B. Kravchenko, Jpn. J. Appl. Phys. 33 (1994) 4907.
[17] J. Hayden, Y. Hayden, J. Campbell, Proc. SPIE 1277 (1990) 121.
[18] T. Minami, J. Mackenzie, J. Am. Ceram. Soc. 60 (1977) 232.
[19] J.S. Wang, E.M. Vogel, E. Snitzer, Opt. Mater 3 (1994) 187.
[20] B.R. Judd, Phys. Rev. 127 (1962) 750.
[21] G.S. Ofelt, J. Chem. Phys. 37 (1962) 511.
[22] S. Tanabe, J. Non-Cryst. Solids 259 (1999) 1.
[23] S. Tanabe, J. Appl. Phys. 73 (1993) 8451.
[24] H. Ebendorff-Heidepriem, D. Ehrt, M. Bettinelli, A. Speghini, J. Non-Cryst. Solids 240 (1998) 66.
[25] L. Pauling, J. Am. Chem. Soc. 51 (1929) 68.
[26] H. Takebe, K. Moringa, T. Izumitani, J. Non-Cryst. Solids 178 (1994) 58.
[27] W.T. Carnal, P.R. Fields, K. Rajnak, J. Chem. Phys. 49 (1968) 4424.
[28] S. Tanabe, T. Hanada, J. Non-Cryst. Solids 196 (1996) 101.
[29] M.J. Weber, Phys. Rev. 157 (1957) 262.
[30] A.A. Kaminskii, Laser Crystals: Their Physics and Properties, Springer-Verlag, New York, 1990.
[31] G.A. Kumar, E. De la Rosa, H. Desirena, Opt. Commun. 260 (2006) 601.
[32] H. Desirena, E. De la Rosa, L.A. Díaz-Torres, G.A. Kumar, Opt. Mater. 28 (2006) 560.
[33] T. Xu, X. Shen, Q. Nei, Y. Gao, Opt. Mater. 28 (2006) 241.
[34] H. Lin, S. Jiang, J Wu, F. Song, N. Peyghambarian, E.Y.B. Pun, J. Phys. D 36 (2003) 812.
[35] R.R. Jacobs, M.J Weber, IEEE J. Quantum Electron. QE-12 (1976) 102.
[36] D.E. McCumber, Phys. Rev. A 134 (1964) A299–A306.
[37] W.J Miniscalco, R.S. Quimby, Opt. Lett. 16 (1991) 258.
[38] W.L. Barnes, R.I. Laming, E.J. Tarbox, P.R. Morkel, IEEE J. Quantum Electron. 27 (1991) 1004.
[39] S. Bor-Chyuan Hwang, T. Jiang, J. Luo, G. Watson, Sorbello, N. Peyghambarian, J. Opt. Soc. Am. B 17 (2000) 833.
[40] L. Zhang, H. Hu, C. Qi, F. Lin, Opt. Mater 17 (2001) 371.
[41] V.P. Gapontsev, S.M. Matitsin, A.A. Isineev, V.B. Kravchenko, Opt. Laser Technol (1982) 189.
[42] J. Yang, S. Dai, S. Li, L. Hu, Z. Jinag, Chin. J. Lumin. 23 (2002) 485.
[43] C.B. Layne, W.H. Lowdermilk, M.J. Weber, Phys. Rev. B 16 (1977) 10.
[44] Q.Y. Zhang, Z.M. Feng, Z.M. Yang, Z.H. Jiang, J. Quant. Spectrose. Radiat. Transer 98 (2006) 167.